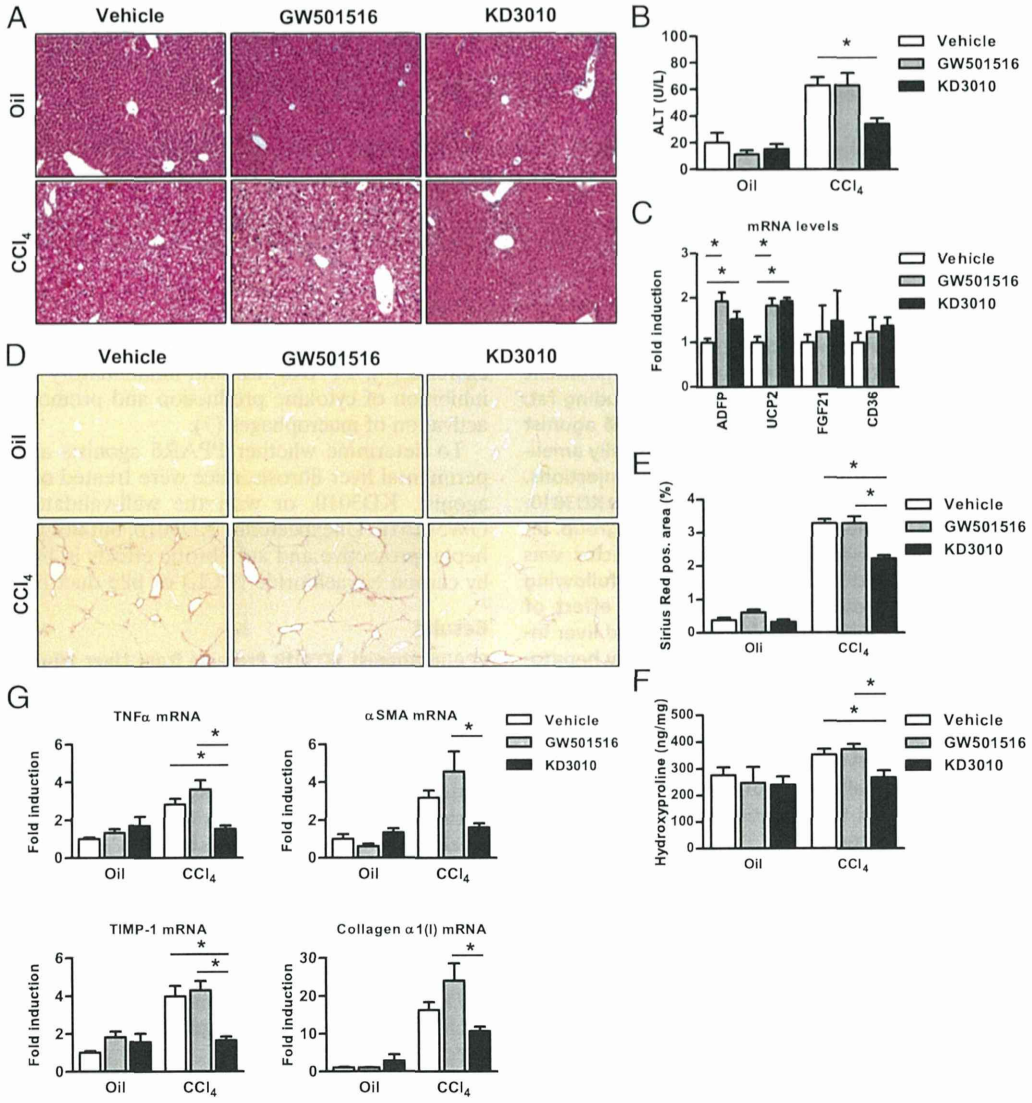

Fig. 1. Reduced liver injury and hepatic fibrosis in mice treated with the PPARδ agonist KD3010. Mice were injected i.p. 12 times with oil as control ($n = 4$ in each group) or with CCl_4 and were administered vehicle ($n = 14$), GW501516 (2 mg/kg; $n = 12$), or KD3010 (10 mg/kg; $n = 11$) daily by oral gavage. (*A*) Representative H&E-stained liver sections are shown. (*B*) ALT levels were measured in the serum of mice. (*C*) Relative gene-expression levels of *ADFP*, *UCP2*, *FGF21*, and *CD36* were determined in the liver of mice treated with vehicle, GW501516, or KD3010 for 5 wk ($n = 4$ in each group). (*D* and *E*) Collagen deposition was evaluated by Sirius Red staining and quantitated by image analysis. Representative sections stained with Sirius Red are shown for vehicle-, GW501516-, and KD3010-treated mice. (*F*) Hydroxyproline content was measured in the liver of mice. (*G*) Hepatic *TNFα*, *αSMA*, *TIMP-1*, or *collagen α1(I)* gene expression was assessed by qPCR. $^*P < 0.05$.

equally impressive reduction of hepatic expression of mRNA encoding *collagen α1(I)* was found in the KD3010 group, and induction of tissue inhibitor of matrix metalloproteinases (*TIMP*)-*1*, an important mediator of liver fibrosis, was decreased in the KD3010 group (Fig. 1*G*). Taken together, PPARδ ligand activation by KD3010, but not by GW501516, protects against chemically induced liver injury and fibrosis and reduces hepatic inflammation.

KD3010 Protects Against Cholestasis-Induced Liver Fibrosis. To determine whether the PPARδ agonist KD3010 suppresses hepatic fibrosis induced by a different etiology, mice underwent cholestatic liver injury by BDL and were treated daily with vehicle or KD3010. Twenty-one days after BDL, liver injury was reduced markedly in the KD3010 group as seen on H&E-stained liver sections (Fig. 2*A*). Mice treated with KD3010 showed a significant reduction in fibrosis as evidenced by Sirius Red staining (Fig. 2 *B* and *C*). The survival rate was significantly higher in PPARδ agonist-treated mice subjected to BDL (Fig. 2*D*). In addition, compared with mice treated with vehicle, the KD3010 BDL group showed decreased expression of inflammatory genes in the liver, including *TNFα* and *IL-1β* (Fig. 2*E*). Consistent with the histopathology, hepatic *TIMP-1* and collagen α1(I) gene expression was decreased following PPARδ ligand activation (Fig. 2*E*). Thus, PPARδ activation protects from both hepatotoxic and cholestatic liver fibrosis.

Cellular Expression of PPARδ in the Liver. To determine which hepatic cells express PPARδ in vivo, we performed double staining for PPARδ and F4/80, as a marker for Kupffer cells, or desmin, as a marker for hepatic stellate cells. PPARδ protein expression was found in the nucleus of Kupffer cells and hepatic stellate cells (Fig. 3*A*). Notably, not all Kupffer cells or hepatic stellate cells expressed PPARδ, consistent with reports of heterogeneous

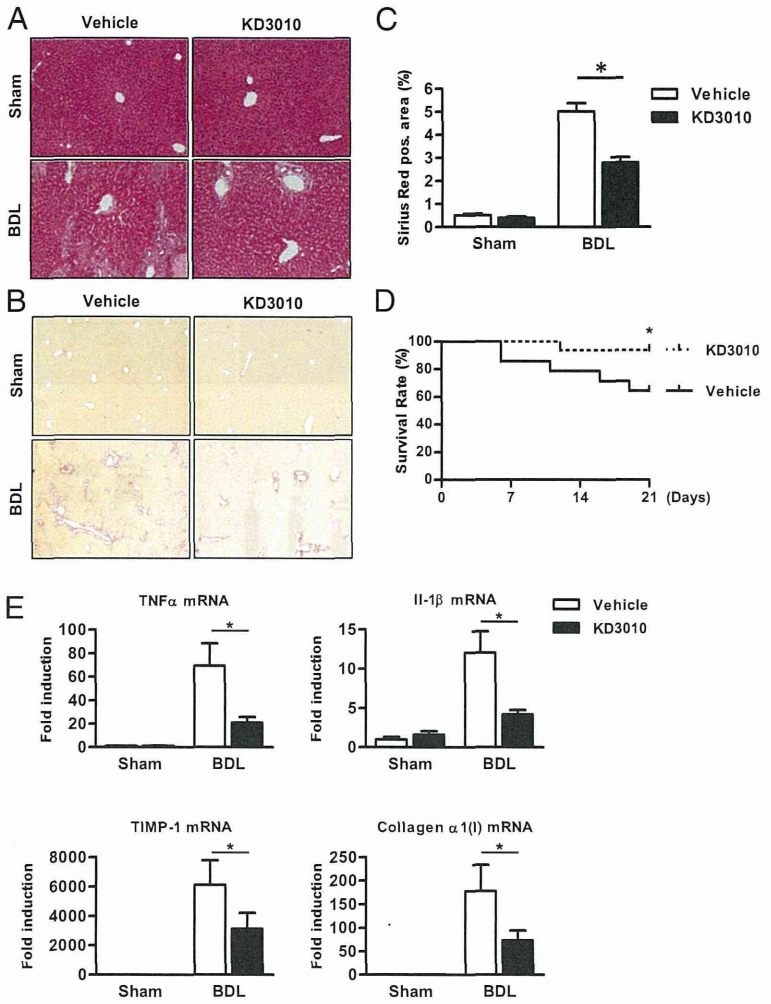

Fig. 2. Mice receiving KD3010 are protected from liver fibrosis after BDL. Mice underwent sham operation ($n = 4$ in each group) or BDL for 21 d and were treated with vehicle ($n = 9$) or KD3010 ($n = 14$). (*A*) Representative H&E-stained liver sections are shown. (*B* and *C*) Hepatic fibrosis was assessed by Sirius Red staining. Representative sections are shown. (*D*) Survival of mice receiving vehicle ($n = 14$) or KD3010 ($n = 16$) following BDL for 21 d. (*E*) Hepatic *TNFα*, *IL-1β*, *TIMP-1*, or *collagen α1(I)* gene expression was assessed by qPCR. $^*P < 0.05$.

Kupffer cell and hepatic stellate cell populations (8). Hepatocytes showed weak positive staining for PPARδ protein. Adipose tissue was used as a positive staining control (Fig. S1).

A similar expression pattern was observed on the gene level. *PPARδ* mRNA was expressed predominantly in Kupffer cells and in hepatic stellate cells isolated from normal liver but was expressed only minimally in hepatocytes (Fig. 3*B*). To confirm the responsiveness of hepatocytes to a PPARδ ligand, hepatocytes were isolated, and expression of PPARδ-responsive genes was determined following treatment with KD3010. KD3010 induced PPARδ-responsive genes such as *ADFP*, pyruvate dehydrogenase kinase, isoenzyme 4 (*PDK4*), and angiopoietin-like 4 (*Angptl4*) but not the PPARα- and PPARγ-responsive genes, *FGF21* and *CD36*, respectively (Fig. 3*C*). These results indicate that KD3010 is capable of activating PPARδ in hepatocytes.

Polarization State of Kupffer Cells Is Not Affected by KD3010. In response to different stimuli, Kupffer cells are capable of differentiating into two polarization states, M1 and M2. LPS promotes Kupffer cell differentiation to a classical, M1 phenotype. The M1 activation pattern is responsible for up-regulating proinflammatory mediators (9). To delineate the effects of KD3010 on Kupffer cells, primary Kupffer cells were isolated from wild-type mice and cultured in the presence of KD3010. The morphology did not change following treatment with KD3010 for 1 d in culture compared with vehicle-treated cells (Fig. S2*A*). KD3010 induced PPARδ-responsive genes such as *ADFP*, *PDK4*, and *Angptl4* in primary Kupffer cells (Fig. 3*D*). LPS-induced expression of *TNFα*, *IL-6*, and *IL-1β* was not suppressed by KD3010 in cultured Kupffer cells (Fig. S2*B*). In contrast, an alternative or M2 phenotype of Kupffer cells is induced in response to IL-4 and IL-13. The M2 phenotype is thought to produce anti-inflammatory factors and to promote tissue repair after inflammation and/or injury (7, 10). IL-4–induced expression of M2 markers such as *arginase1* and macrophage galactose-type C-type lectin 1 (*Mgl-1*) was not affected following KD3010 treatment in cultured Kupffer cells (Fig. S2*B*). Thus, KD3010 induces a common set of PPARδ target genes such as *ADFP*, *PDK4*, and *Angptl4* in both M1 and M2 Kupffer cells.

PPARδ Ligand KD3010 Does Not Decrease the Activation and Fibrogenic Potential of Hepatic Stellate Cells. To explain the beneficial effect of KD3010 in liver fibrosis, we next focused on hepatic stellate cells. Hepatic stellate cells isolated from wild-type mice did not change their morphology following treatment with

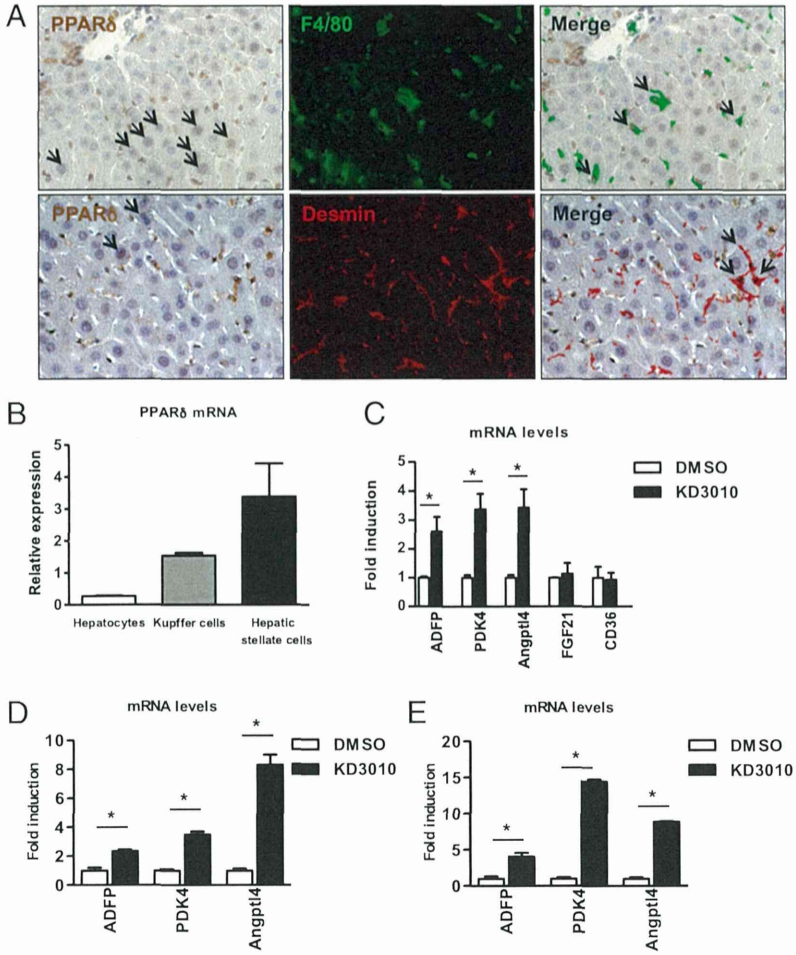

Fig. 3. Hepatocytes express PPARδ. (*A*) Immunohistochemical staining for PPARδ (brown), and immunofluorescent staining for F4/80 (green) and desmin (red) was performed to detect PPARδ protein in Kupffer cells and hepatic stellate cells, respectively. Black arrows indicate positively stained hepatocytes (*Left*), double-positive Kupffer cells (*Upper Right*), and hepatic stellate cells (*Lower Right*). (*B*) Liver cell fractions were isolated from a normal liver. PPARδ mRNA was analyzed by qPCR and normalized to 18S. The mean of three independent isolations is shown. (*C*) Hepatocytes were cultured with DMSO or KD3010 (5 μM). Gene expression of *ADFP*, pyruvate dehydrogenase kinase, isoenzyme 4 (*PDK4*), angiopoietin-like 4 (*Angptl4*), fibroblast growth factor (*FGF*)-*21*, and *CD36* was analyzed by qPCR and normalized to 18S. The mean of four independent experiments are shown. (*D*) Kupffer cells were cultured with DMSO or KD3010 (1 μM). Gene expression of *ADFP*, *PDK4*, and *Angptl4* was analyzed by qPCR and normalized to 18S. (*E*) Hepatic stellate cells were cultured with DMSO or KD3010 (1 μM). Gene expression of *ADFP*, *PDK4*, and *Angptl4* was analyzed by qPCR and normalized to 18S. $*P < 0.05$.

KD3010 for 3 d in culture compared with vehicle-treated cells (Fig. S3*A*). Although KD3010 induced PPARδ-responsive genes such as *ADFP*, *PDK4*, and *Angptl4* (Fig. 3*E*), hepatic stellate cells incubated with KD3010 showed no change in the expression of fibrogenic genes *αSMA*, *TIMP-1*, and *collagen α1(I)* or the proliferation marker *cyclin D1* (Fig. S3*B*). *Hepatocyte growth factor* (*HGF*) was induced in KD3010-treated hepatic stellate cells compared with control cells (Fig. S3*B*). Thus, KD3010 does not modulate fibrogenic properties of hepatic stellate cells.

PPARδ Ligand Activation Protects Hepatocytes from Starvation and CCl_4-Induced Cell Death. We then focused on hepatocytes as potential targets for the beneficial effect of KD3010 in liver injury and fibrosis. KD3010 protected cultured hepatocytes from starvation-induced cytotoxicity, as evidenced by reduced ALT in the supernatant and reduced cell death (released LDH) (Fig. 4 *A*–*C*). In addition, KD3010 protected cultured hepatocytes from CCl_4-induced cell death, as assessed by diminished propidium iodide (PI) staining (Fig. 4*D*), and reduced ALT levels in the supernatant (Fig. 4*E*). The hepatoprotective effect of KD3010 was absent in PPARδ-deficient hepatocytes (Fig. 4*E*), demonstrating that the hepatoprotection of KD3010 is not an off-target effect.

Because reduced oxidative stress might mediate the protection from cell death, reactive oxygen species (ROS) were measured and indeed were lower in CCl_4-treated hepatocytes incubated with KD3010, whereas hepatocytes incubated with GW501516 showed more ROS production (Fig. 4*F*). KD3010 treatment of wild-type hepatocytes decreased thiobarbituric acid-reactive substances (TBARS), a measure of lipid peroxidation, after CCl_4 exposure, but this effect was not seen in PPARδ-deficient hepatocytes (Fig. 4*G*). We next examined cytochrome P450 (Cyp) expression, because its function is to catalyze the oxidation of organic substances. Gene expression of several Cyp family members was induced following incubation with KD3010. However, *Cyp2E1*, the CCl_4-metabolizing enzyme, was not affected by KD3010 (Fig. 4*H*). Thus, KD3010 induces Cyp family members, decreases ROS in hepatocytes, and protects hepatocytes from starvation and toxic cell death.

To explain further the differences between KD3010 and GW501516, we compared the gene-activation profile of the two compounds in cultured hepatocytes by gene-expression micro-

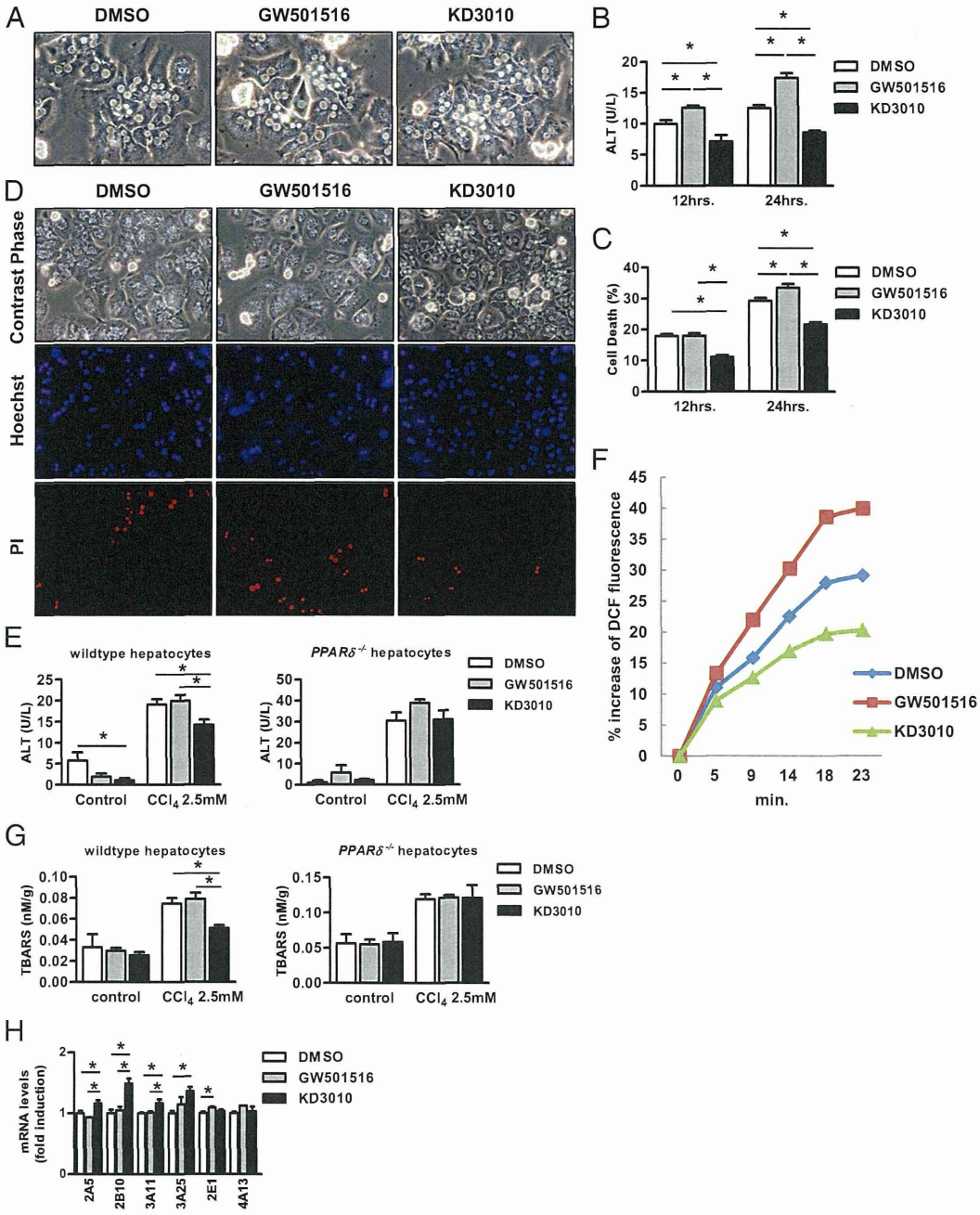

Fig. 4. KD3010 protects hepatocytes from cell death in culture. Hepatocytes were cultured in KRB without glucose and without FCS for indicated time periods in the presence of DMSO, GW501516 (100 nM), or KD3010 (5 μM). (*A*) Representative photomicrographs are shown. ALT was measured in the supernatant of cells (*B*), and cell death was assessed (C). (*D*) CCl_4 (2.5 mM) was added to hepatocytes after 12 h in the presence of DMSO, GW501516 (100nM) or KD3010 (5 μM). Representative photomicrographs of cells and Hoechst- and PI-stained hepatocytes are shown. (*E*) CCl_4-induced cell death was assessed in wild-type and PPARδ-deficient hepatocytes by measuring ALT in the supernatant. (*F*) Hepatocytes cultured with DMSO, GW501516 (100 nM), or KD3010 (5 μM) for 12 h were loaded with redox-sensitive dye CM-H_2DCFDA (10 μM) for 20 min. Fluorescent signals were quantified continuously for 23 min using a fluorometer. (*G*) TBARS were assessed in wild-type and PPARδ-deficient hepatocytes. (*H*) Hepatocytes were cultured in KRB in the presence of DMSO, GW501516 (100 nM) or KD3010 (5 μM) for 12 h. qRT-PCR was performed for Cyp family members. Results shown are the mean of four different hepatocyte isolations.*$P < 0.05$.

array analysis. Surprisingly, the two PPARδ agonists had distinct gene-expression profiles (Fig. S4 *A–C* and Tables S1 and S2). Known PPARδ-responsive genes such as *PDK4* and carnitine palmitoyltransferase 2 were induced by both agonists. KD3010 caused a larger change in gene expression than did GW501516. Interestingly, connective tissue growth factor (*CTGF*) was induced by GW501516 but not by KD3010. We therefore compared hepatic *CTGF* gene expression following CCl_4 treatment in mice gavaged with GW501516 or KD3010. Similar to the in vitro results, *CTGF* mRNA was significantly higher in GW501516-treated than in vehicle-treated mice, but there was no difference between KD3010- and vehicle-treated mice following repeated CCl_4 injections (Fig. S4*D*). CTGF has potent profibrogenic properties and is produced and secreted by hepatocytes (11). Recently CTGF has been shown to be induced by p53 in hepatocytes and to result in liver fibrosis (12), possibly

thereby contributing to the different effects on liver fibrosis observed with GW501516 and KD3010.

Discussion

To address the effect of PPARδ activation on chronic liver diseases, we took an unbiased approach to test a potent and highly selective PPARδ agonist, KD3010, in mouse models of liver fibrosis induced by hepatotoxicity (CCl_4 injections) and cholestasis (BDL). KD3010 shows dramatic antifibrotic effects in vivo and was more effective than the well-validated PPARδ agonist GW501516. Hepatocytes appear to be the target for PPARδ ligand activation, because KD3010 protects cultured hepatocytes from starvation- and CCl_4-induced cell death. Thus, a hepatoprotective effect upon ligand activation mediates the beneficial effect of KD3010 in experimental animal models of liver fibrosis.

The role of PPRAδ in chronic liver disease has not been examined previously. PPARδ deficiency increases acute liver toxicity induced by azoxymethane or CCl_4 in mice (13), whereas treatment with the PPARδ ligand GW0742 ameliorates acute CCl_4-induced liver toxicity in a PPARδ-dependent fashion (14). The cellular mechanism was not identified in these studies (13). In contrast to the beneficial effect of PPARδ ligand activation in acute liver disease, enhanced acute liver toxicity after one dose of CCl_4 was reported to occur in rats when another PPARδ ligand, L165041, was administered concomitantly (15). Our study demonstrates that a highly specific PPARδ agonist, KD3010, showed potent beneficial effects in two models of liver injury and fibrosis, whereas the known PPARδ agonist GW501516 did not affect chronic liver injury. Consistent with our results, GW501516 did not affect liver fibrosis in a choline-deficient, ethionine-supplemented mouse model of steatohepatitis (16). Differences in the physiological outcomes of specifically targeted nuclear receptor pharmacophores are well documented in the steroid receptor family for estrogens, glucocorticoids, and androgens. In addition, differential outcomes have been reported recently for targeted synthetic farnesoid X receptor ligands, as demonstrated by global gene-expression profiles (17). The differences reported here for the PPARδ agonists can be attributed to a number of different factors, including different specificities for other PPAR isoforms, potencies of different synthetic compounds, and in vivo pharmacological properties of the compounds including differential tissue distribution, degradation, and clearance. This study demonstrates that distinct structural pharmacophores, although classified as agonists, can confer widely differing benefits in the pathological setting when studying the effects of nuclear receptor-targeted agonists.

PPARδ plays an important role in energy, glucose, and lipid homeostasis. This role may be mediated in part by alternative M2 activation of macrophages/Kupffer cells. Genetic ablation of PPARδ in bone marrow cells impairs alternative activation of tissue macrophages and predisposes mice to the development of insulin resistance and metabolic syndrome, including adiposity and hepatic steatosis on a high-fat diet (7). PPARδ is induced by T-helper type 2 cytokines derived from hepatocytes or adipocytes to induce alternative activation of adipose tissue macrophages or Kupffer cells, suggesting that M2 macrophages have a profound influence on oxidative metabolism and lipid homeostasis. Alternatively activated macrophages attenuate inflammation in the liver and also in white fat tissue (7, 10). In contrast, recent studies do not support a role for alternative activation of macrophages mediated by PPARδ. Loss of PPARδ in bone marrow-derived cells did not affect glucose tolerance in mice fed a high-fat diet (18). PPARγ, but not PPARδ, activation promotes human monocyte differentiation toward alternative macrophages (19). Although Kupffer cells express endogenous PPARδ, our study provides evidence that Kupffer cells are not an important target for PPARδ ligand activation to mediate its antifibrotic effect. KD3010 did not modulate in vitro activation and the polarization state of Kupffer cells. Hepatic stellate cells, the main cell type producing extracellular matrix in liver fibrosis, express endogenous PPARδ, but their fibrogenic properties are not changed following PPARδ activation in vitro.

Hepatocytes, the predominant liver cell type, express PPARδ and induce PPARδ-responsive genes upon KD3010 treatment. KD3010, but not GW501516, protects cultured hepatocytes from starvation- and CCl_4-induced cell death. In fact, GW501516 increased ROS production and starvation-induced cell death in cultured hepatocytes. KD3010-mediated cytoprotection is PPARδ dependent, because the effect is lost in PPARδ-deficient hepatocytes. The mechanism likely involves expression of Cyp enzymes, which are stimulated by KD3010 and result in oxidation and detoxification of organic substances, whereas GW501516 did not alter expression of Cyp enzymes. In addition to the PPARδ-dependent cytoprotective effect, we also demonstrate the induction of CTGF by GW501516, which is a strong profibrotic cytokine. Combined, the cytoprotection and the absence of a profibrogenic cytokine confer protection against fibrosis and explain the differences between KD3010 and GW501516 observed in our study. Our study identifies hepatocytes as the main target cell population in the liver that mediates the beneficial effect of KD3010 in a PPARδ-dependent fashion.

Chronic liver disease results in hepatic fibrosis. The only current treatment paradigm for patients with hepatic fibrosis is treatment of the underlying liver disease (20). If the causative agent cannot be removed, there are currently no effective antifibrotic treatments for patients with chronic liver diseases (21). Experimental studies in rodents have revealed targets to prevent the progression of fibrosis. However, the efficacy of most treatments has not been tested in humans. Additionally, promising targets identified in rodents may result in undesirable side effects in humans. For example, inhibition of the profibrotic cytokine TGFβ-1 may favor cancer development, especially in liver cirrhosis, which is a premalignant state (2). On the other hand, PPARδ deficiency results in azoxymethane-induced regenerative liver cell hyperplasia, suggesting that PPARδ protects against enhanced cell proliferation in the liver (13). Insights into the mechanisms of the development of hepatic fibrosis provide an opportunity to develop therapeutic interventions for human clinical use. A PPARδ agonist may serve as a treatment option for liver fibrosis. The findings reported here should promote further clinical investigation into the potential use of a PPARδ agonist in treating patients with chronic liver diseases.

Materials and Methods

Mouse Models of Liver Fibrosis. Male 11-wk-old C57/B6 mice were treated with CCl_4 (2 μL/g body weight; 1:4 dilution with corn oil) or with corn oil as control (2 μL/g body weight) by i.p. injection every third day. Injections were repeated for a total of 12 times. Livers were harvested 3 d after the last injection. BDL or sham operation as control was performed as described previously (22), and livers were harvested 21 d later. All animal procedures were performed under the guidelines set by The University of California, San Diego Institutional Animal Care and Use Committee and are in accordance with those set by the National Institutes of Health.

Treatment Protocol. KD3010 (chemical name (S)-4-[cis-2,6-dimethyl-4-(4-trifluoromethoxy-phenyl)piperazine-1-sulfonyl]-indan-2-carboxylic acid tosylate) (Fig. S5) is a potent, orally active, and selective PPARδ agonist (Kalypsys Inc.). Phase I clinical trials have successfully been completed in healthy volunteers and demonstrated safety and tolerability without clinically relevant treatment- or dose-related trends in the laboratory, vital sign, ECG, or physical examination safety parameters (www.kalypsys.com). KD3010 has no appreciable interaction with human, rhesus, or murine PPARα and PPARγ receptors, as evidenced by EC_{50} values in excess of 7–10 μM. Cell-based reporter gene assays indicate that KD3010 (up to 10 μM) does not affect the function of mouse/human pregnane X receptor and human constitutive androstane receptor. For in vitro experiments we used concentrations of 1–5 μM. Mean plasma compound concentration of mice treated with CCl_4 and gavaged with KD3010 was 4 ± 0.8 μM (at time of harvesting). Mice were assigned randomly into groups at the beginning of the study. The study was conducted in a blinded fashion, and the researchers performing the in vivo

experiments (CCl_4 treatment and BDL; Figs. 1 and 2) remained blinded to the nature of the experimental drugs until all data were analyzed. Mice were treated daily with vehicle or KD3010 (10 mg/kg) by oral gavage. At times of CCl_4 injections, the compounds were administered 2 h after the last gavage was given. Similarly, a well-characterized PPARδ agonist GW501516 (2 mg/kg) or vehicle was administered to mice daily by gavage (6).

Liver Enzymes and Staining Procedures. Blood was taken at the time of harvesting. ALT in the plasma was measured by the Infinity kit (Thermo Fisher Scientific) according to the manufacturer's instructions. Formalin-fixed liver samples were embedded in paraffin and stained with H&E. Sirius Red staining [saturated picric acid containing 0.1% (wt/vol) Direct Red 80] was performed as described (22). The Sirius Red-positive area was measured at a final magnification of 40×. The entire median lobe of the liver was imaged, and 6–14 images per animal were taken and analyzed using National Institutes of Health Image J. The results are presented as percentage area positively stained for Sirius Red. Immunohistochemistry and immunofluorescence were performed using anti-PPARδ antibody (1:100; Santa Cruz), anti-desmin antibody (1:200; DAKO), and anti-F4/80 antibody (1:200; eBioscience) as described (22).

Hydroxyproline Measurement. Liver tissue was homogenized in ice-cold distilled water (900 μL) using a Power Gen homogenizer (Fisher). Subsequently, 125 μL of 50% (wt/vol) trichloroacetic acid was added, and the homogenates were incubated further on ice for 20 min. Precipitated pellets were hydrolyzed for 18 h at 110 °C in 6N HCL. After hydrolysis, the samples were filtered and neutralized with 10N NaOH, and the hydrolysates were oxidized with Chloramine-T (Sigma) for 25 min at room temperature. The reaction mixture then was incubated in Ehrlich's perchloric acid solution at 65 °C for 20 min and cooled to room temperature. Sample absorbance was measured at 560 nm in duplicate. Purified hydroxyproline (Sigma) was used to set a standard. Hydroxyproline content was expressed as nanogram of hydroxyproline per milligram liver.

Gene-Expression Analysis. Total RNA was extracted with TRIZOL (Invitrogen). RNA was digested with DNase using the DNA-free kit (Ambion). DNase-treated RNA was reverse transcribed using the High Capacity cDNA Reverse Transcription kit (ABI). Real-time quantitative PCR (qPCR) was performed for 40 cycles of 15 s at 95 °C and 60 s at 60 °C using an ABI 7000 sequence detection system. The relative abundance of the target genes was obtained by calculating against a standard curve and normalized to 18S or cyclophilin as internal control. Probes purchased from ABI or primers from the National Institutes of Health mouse qprimer depot were used with SYBR green (Bio-Rad). Microarrays were performed as described (6). Briefly, samples were labeled and hybridized to Affymetrix Mouse Genome 430 2.0 arrays ($n = 3$ in each group). Microarray data have been deposited in the Gene Expression Omnibus (accession code GSE32121). Microarray data analysis was performed as described (23). In brief, image data were converted into nonnormalized sample probe profiles using the BeadStudio software (Illumina) and analyzed on the VAMPIRE microarray analysis framework48. We constructed stable variance models for each of the two experimental conditions and identified differentially expressed probes using the unpaired VAMPIRE significance test with a two-sided, Bonferroni-corrected threshold (α_{Bonf}) of 0.05. The VAMPIRE statistical test is a Bayesian statistical method that computes a model-based estimate of noise at each level of gene expression. This estimate then was used to assess the statistical significance of the apparent differences in gene expression in the two experimental conditions.

Isolation and Culture of Hepatocytes, Kupffer Cells, and Hepatic Stellate Cells. Isolation of liver-cell fractions from normal liver using magnetic cell sorting (MACS) has been described (22). Kupffer cells and hepatic stellate cells were isolated from mice by two-step collagenase–pronase perfusion followed by three-layer discontinuous density gradient centrifugation with 8.2% (wt/vol) and 14.5% (wt/vol) Nycodenz (Accurate Chemical and Scientific Corporation) to obtain Kupffer-cell and hepatic stellate-cell fractions. Hepatic stellate cells were collected between the 0 and 8.2% (wt/vol) layer. The Kupffer-cell fraction was selected negatively by MACS using anti-LSEC Micro Beads (Miltenyi Biotech). Kupffer cells were cultured with DMSO or KD3010 (1 μM) for 1 d before stimulation by LPS (1 ng/mL for 4 h) or IL-4 (10 ng/mL for 24 h). Hepatic stellate cells were cultured with DMSO or KD3010 (5μM) for 3 d before harvesting. To induce starvation-associated cell death, hepatocytes were cultured in Waymouth's medium containing 10% (vol/vol) FCS for 3.5 h; Waymouth's medium then was changed to Krebs–Ringer buffer without glucose (KRB) in the presence of DMSO, KD3010 (5 μM), or GW501516 (100 nM). In some experiments, CCl_4 (2.5 mM) was added to hepatocytes after 12 h. Cell death was assessed by measuring ALT in the supernatant, by using a Cytotoxicity Detection Kit (Roche), or by staining with PI. Hepatocytes were isolated from wild-type or PPARδ-deficient mice (4) and were cultured in 96-well black-bottomed plates in KRB for 12 h in the presence of DMSO, KD3010 (5 μM), or GW501516 (100 nM). Cells were loaded with the redox-sensitive dye CM-H_2DCFDA (10 μM) diluted in KRB for 20 min at 37 °C. Cells then were rinsed twice with KRB and stimulated with CCl_4 (2.5 mM). CM-H_2DCFDA fluorescence was detected at excitation and emission wavelengths of 488 nm and 520 nm, respectively. ROS formation was measured in a time course of 23 min using a multiwell fluorescence scanner (Fluostar Optima; BMG Labtech). TBARS were measured by using OxiSelect TBARS Assay Kit (MDA Quantitation). For microarray analysis, RNA was extracted from hepatocytes cultured in Waymouth's medium containing 10% (vol/vol) FCS in the presence of DMSO, KD3010 (5 mM), or GW501516 (100 nM) for 12 h.

Statistical Analysis. Results are reported as mean ± SEM, unless otherwise stated. Comparisons among multiple groups were performed by one-way ANOVA with post hoc test (Tukey's Multiple Comparison Test). Mouse survival data were analyzed statistically by using the Log-rank (Mantel–Cox) test. Comparisons between two groups were performed by the Mann–Whitney *u*-statistic test. $P < 0.05$ was considered statistically significant. All statistical analyses were performed using GraphPad Prism.

ACKNOWLEDGMENTS. KD3010 was provided as a gift from Kalypsys, Inc. This study was supported in part by National Institutes of Health Grants K08 DK081830 and R01 AA020703 (to B.S.), R01 DK072237 (to D.A.B.), R01 DK057978 (to R.M.E.), and R24 DK090962 (to D.A.B. and R.M.E.). This study also was supported by University of California, San Diego Digestive Diseases Research Development Center Grant DK080506 (to B.S.) and by Award K12-HD000850 from the Eunice Kennedy Shriver National Institute of Child Health and Human Development (to E.Y.). R.M.E. was supported by the Helmsley Charitable Trust and by the Howard Hughes Medical Institute. R.M.E. is an investigator of the Howard Hughes Medical Institute and March of Dimes Chair in Molecular and Developmental Biology at the Salk Institute. E.Y. is a Fellow of the Pediatric Scientist Development Program.

1. Bataller R, Brenner DA (2005) Liver fibrosis. *J Clin Invest* 115:209–218.
2. Schnabl B, Scholten D, Brenner DA (2008) What is the potential role of antifibrotic agents for the treatment of liver disease? *Nat Clin Pract Gastroenterol Hepatol* 5: 496–497.
3. Barish GD, Narkar VA, Evans RM (2006) PPAR delta: A dagger in the heart of the metabolic syndrome. *J Clin Invest* 116:590–597.
4. Lee CH, et al. (2006) PPARdelta regulates glucose metabolism and insulin sensitivity. *Proc Natl Acad Sci USA* 103:3444–3449.
5. Oliver WR, Jr., et al. (2001) A selective peroxisome proliferator-activated receptor delta agonist promotes reverse cholesterol transport. *Proc Natl Acad Sci USA* 98: 5306–5311.
6. Narkar VA, et al. (2008) AMPK and PPARdelta agonists are exercise mimetics. *Cell* 134: 405–415.
7. Odegaard JI, et al. (2008) Alternative M2 activation of Kupffer cells by PPARdelta ameliorates obesity-induced insulin resistance. *Cell Metab* 7:496–507.
8. Magness ST, Bataller R, Yang L, Brenner DA (2004) A dual reporter gene transgenic mouse demonstrates heterogeneity in hepatic fibrogenic cell populations. *Hepatology* 40:1151–1159.
9. Olefsky JM, Glass CK (2010) Macrophages, inflammation, and insulin resistance. *Annu Rev Physiol* 72:219–246.
10. Kang K, et al. (2008) Adipocyte-derived Th2 cytokines and myeloid PPARdelta regulate macrophage polarization and insulin sensitivity. *Cell Metab* 7:485–495.
11. Gressner OA, Gressner AM (2008) Connective tissue growth factor: A fibrogenic master switch in fibrotic liver diseases. *Liver Int* 28:1065–1079.
12. Kodama T, et al. (2011) Increases in p53 expression induce CTGF synthesis by mouse and human hepatocytes and result in liver fibrosis in mice. *J Clin Invest* 121:3343–3356.
13. Shan W, et al. (2008) Peroxisome proliferator-activated receptor-beta/delta protects against chemically induced liver toxicity in mice. *Hepatology* 47:225–235.
14. Shan W, et al. (2008) Ligand activation of peroxisome proliferator-activated receptor beta/delta (PPARbeta/delta) attenuates carbon tetrachloride hepatotoxicity by downregulating proinflammatory gene expression. *Toxicol Sci* 105:418–428.
15. Hellemans K, et al. (2003) Peroxisome proliferator-activated receptor-beta signaling contributes to enhanced proliferation of hepatic stellate cells. *Gastroenterology* 124: 184–201.
16. Knight B, Yeap BB, Yeoh GC, Olynyk JK (2005) Inhibition of adult liver progenitor (oval) cell growth and viability by an agonist of the peroxisome proliferator activated receptor (PPAR) family member gamma, but not alpha or delta. *Carcinogenesis* 26: 1782–1792.
17. Downes M, et al. (2003) A chemical, genetic, and structural analysis of the nuclear bile acid receptor FXR. *Mol Cell* 11:1079–1092.

18. Marathe C, et al. (2009) Preserved glucose tolerance in high-fat-fed C57BL/6 mice transplanted with PPARgamma-/-, PPARdelta-/-, PPARgammadelta-/-, or LXRalphabeta-/- bone marrow. *J Lipid Res* 50:214–224.
19. Bouhlel MA, et al. (2009) Unlike PPARgamma, PPARalpha or PPARbeta/delta activation does not promote human monocyte differentiation toward alternative macrophages. *Biochem Biophys Res Commun* 386:459–462.
20. Poynard T, et al. (2002) Impact of pegylated interferon alfa-2b and ribavirin on liver fibrosis in patients with chronic hepatitis C. *Gastroenterology* 122:1303–1313.
21. Di Bisceglie AM, et al.; HALT-C Trial Investigators (2008) Prolonged therapy of advanced chronic hepatitis C with low-dose peginterferon. *N Engl J Med* 359: 2429–2441.
22. Taura K, et al. (2008) Hepatic stellate cells secrete angiopoietin 1 that induces angiogenesis in liver fibrosis. *Gastroenterology* 135:1729–1738.
23. Pei L, et al. (2011) Thyroid hormone receptor repression is linked to type I pneumocyte-associated respiratory distress syndrome. *Nat Med* 17:1466–1472.

Journal of Gastroenterology and Hepatology

JGHF

doi:10.1111/j.1440-1746.2011.07002.x

NOVEL INSIGHTS INTO LIVER AND PANCREATIC FIBROGENESIS

What's new in liver fibrosis? The origin of myofibroblasts in liver fibrosis

Keiko Iwaisako, David A Brenner and Tatiana Kisseleva

Department of Medicine, University of California, San Diego, La Jolla, California, USA

David A Brenner

Key words
hepatic stellate cell, liver fibrosis, myofibroblast, portal fibroblast.

Accepted for publication 11 November 2011.

Abstract

Chronic liver injury of many etiologies produces liver fibrosis and may eventually lead to the formation of cirrhosis. Fibrosis is part of a dynamic process associated with the continuous deposition and resorption of extracellular matrix, mainly fibrillar collagen. Studies of fibrogenesis conducted in many organs including the liver demonstrate that the primary source of the extracellular matrix in fibrosis is the myofibroblast. Hepatic myofibroblasts are not present in the normal liver but transdifferentiate from heterogeneous cell populations in response to a variety of fibrogenic stimuli. Debate still exists regarding the origin of hepatic myofibroblasts. It is considered that hepatic stellate cells and portal fibroblasts have fibrogenic potential and are the major origin of hepatic myofibroblasts. Depending on the primary site of injury the fibrosis may be present in the hepatic parenchyma as seen in chronic hepatitis or may be restricted to the portal areas as in most biliary diseases. It is suggested that hepatic injury of different etiology triggers the transdifferentiation to myofibroblasts from distinct cell populations. Here we discuss the origin and fate of myofibroblast in liver fibrosis.

Correspondence
Professor David A Brenner, Division of Gastroenterology, Department of Medicine, School of Medicine, University of California, San Diego, 9500 Gilman Drive #0602, Biomedical Sciences Building 1318, La Jolla, CA 92093-0602, USA. Email: dbrenner@ucsd.edu

Conflict of Interests: There are no conflicts of interests.

Introduction

Liver fibrosis results from continuous injury to the liver, including viral hepatitis, alcohol abuse, metabolic diseases, autoimmune diseases, and cholestatic liver diseases. In other words, fibrosis is a consequence of the excessive healing response triggered by chronic liver injury. The end stage of liver fibrosis, cirrhosis, is histologically characterized by increased deposition and altered composition of the extracellular matrix (ECM) and the appearance of regenerative nodules.[1] The destruction of the normal architecture and the loss of hepatocytes prevent the liver from its normal synthetic and metabolic function. Thus, the fibrogenic evolution progresses to cirrhosis, liver failure, and hepatocellular cancer.[2] There is increasing evidence that the hepatic fibrosis is reversible if the stimuli are successfully removed.[3] However, only subsets of liver diseases are treated effectively, and there are no specific treatments for liver fibrosis. An ideal anti-fibrogenic therapy would be liver-specific and effective in attenuating excessive ECM deposition.[4]

In all clinical and experimental liver fibrosis, myofibroblasts are the source of the ECM constituting the fibrous scar. Myofibroblasts are only found in the injured, but not the normal, liver. Thus, the activated myofibroblast is a pivotal player in development of liver cirrhosis, and has recently attracted interest as a therapeutic target. However, the origin of the hepatic myofibroblast is still unclear, and perhaps the fibrosis induced by different types of liver injury results from different fibrogenic cells. Hepatic myofibroblasts may originate from bone marrow-derived mesenchymal cells and fibrocytes,[5] but only a small contribution of BM derived cells to the myofibroblast population has been detected in experimental liver fibrosis. Another mechanism implicated in fibrogenesis is the epithelial-to-mesenchymal transition (EMT), in which epithelial cells acquire features of mesenchymal cells and may give rise to fully differentiated myofibroblasts.[6,7] However, recent cell fate mapping studies have failed to detect any hepatic myofibroblasts originating from hepatocytes, cholangiocytes, or epithelial progenitor cells. Endothelial-to-mesenchymal transition (EndMT), when endothelial cells undergo a similar phenotypic change to myofibroblasts[8,9] is a theoretically, but not yet assessed source of liver myofibroblasts. Thus, the major sources of myofibroblasts in liver fibrosis appear to be the endogenous liver mesenchymal cells, the hepatic stellate cells and the portal fibroblasts.

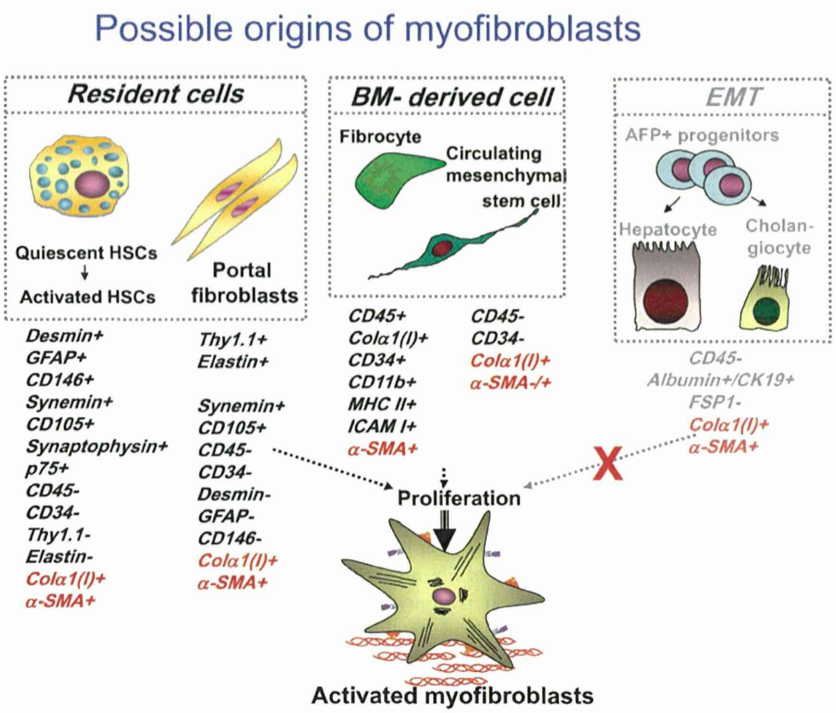

Figure 1 The proposed sources of hepatic myofibroblasts: resident cells (hepatic stellate cells and portal fibroblasts); bone marrow (BM)-derived mesenchymal cells, and cells originated by epithelial-to-mesenchymal transition. Modified from Bataller *et al.*[1]

Myofibroblasts

The origin of fibrogenic hepatic myofibroblasts has been intensively discussed and investigated, and several sources of myofibroblasts have been identified[10–13] (Fig. 1). In the fibrotic liver, hepatic stellate cells (HSCs) have been reported to mainly contribute to the collagen producing cells.[1] Therefore, HSCs are currently considered to be the major, but not the only, source of hepatic myofibroblasts in liver injury.[14]

Myofibroblasts are characterized by a stellate shape and expression of specific markers.[15] In response to fibrogenic stimuli, pro-fibrogenic cells are converted to myofibroblasts. They express α-smooth muscle actin (α-SMA), secrete ECM (e.g. collagen type I and III, fibronectin) and are highly contractile.[14] Classical myofibroblasts differentiate from a mesenchymal lineage and, therefore, lack expression of lymphoid markers such as CD45 or CD34.

The origins of myofibroblasts

Hepatic stellate cells

Hepatic stellate cells (HSCs) are perisinusoidal cells that normally reside in the space of Disse and have stored lipid droplets.[2,16] Under normal conditions, HSCs are present in the space of Disse and exhibit a quiescent phenotype. HSCs express neural markers, such as glial fibrilar acidic protein (GFAP), synemin, synaptophysin,[1] and nerve growth factor receptor p75,[17,18] desmin, secrete HGF, and store vitamin A in lipid droplets.[19] In response to chronic liver injury, quiescent HSCs are activated, release vitamin A and acquire contractility. Upon activation, HSCs change their morphology to become myofibroblasts, migrate to the site of injury, downregulate neural markers and upregulate mesenchymal markers, (e.g. collagen α1(I), α-SMA, and fibronectin).

Portal fibroblasts

Portal fibroblasts are spindle shaped cells that are present in the portal area. Under normal conditions, they participate in physiological ECM turnover[14,20–22] and do not express α-SMA. It is induced mostly by cholestatic liver injury,[23] that portal fibroblasts proliferate[24] and secrete collagen around portal tracts.[25] Portal fibroblasts are distinct from HSCs in that they do not have vitamin A droplets, but express elastin and Thy-1.1 (a glycophosphatidylinositol-linked glycoprotein of the outer membrane leaflet described in fibroblasts of several organs).[26,27] A proteomics study demonstrated that myofibroblasts derived from portal mesenchymal cells express much higher levels of cofilin-1 than activated HSCs. Portal fibroblasts do not express cytoglobin,[28] desmin or GFAP, so that these markers are useful to identify myofibroblasts derived from HSCs. In chronic cholestatic disorders, the fibrosis is initially located around portal tracts (Fig. 2). The histological findings of liver fibrosis combined with immunohistochemistry using these specific markers demonstrate that portal fibroblasts contribute to myofibroblasts in cholestatic liver injury.[1]

Born marrow derived mesenchymal cells

Born marrow (BM)-derived mesenchymal cells can also differentiate into myofibroblasts.[29,30] Myofbroblasts originated from BM-derived mesenchymal cells are seen in fibrotic lungs[31] and liver,[30] and contribute to fibrogenesis.[2,30,32] By fractionating the BM stem cell compartment, hepatic BM-derived mesenchymal stem cells (MSCs)[30,31] may differentiate into hepatic myofibroblasts. MSCs are defined as self-renewable, multipotent progenitor cells with the capacity to differentiate into lineage specific cells that form bone, cartilage, fat, tendon and muscle.[33,34] Unlike hematopoietic stem cells, MSCs are more radio-resistant[35] and reside mostly in

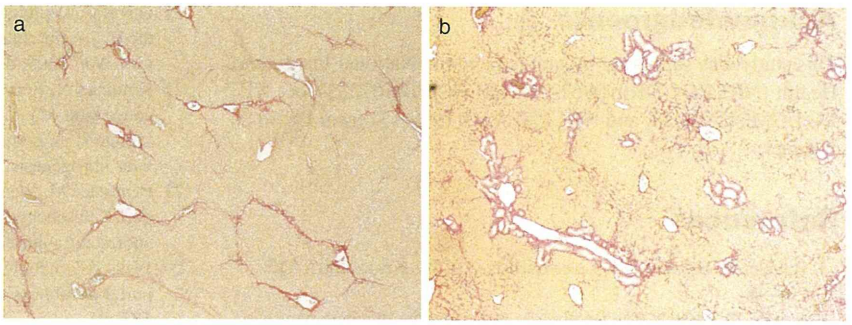

Figure 2 Liver fibrosis induced by hepatotoxic injury or cholestatic injury in mice. Liver sections were assessed by Sirius red staining. (a) Hepatotoxic injury model; the fibrotic tissue is initially located in pericentral and perisinusoidal areas. In advance, collagen bands to bridging fibrosis to frank cirrhosis occurs. (b) Cholestatic injury model; the fibrotic tissue is initially located around portal tracts.

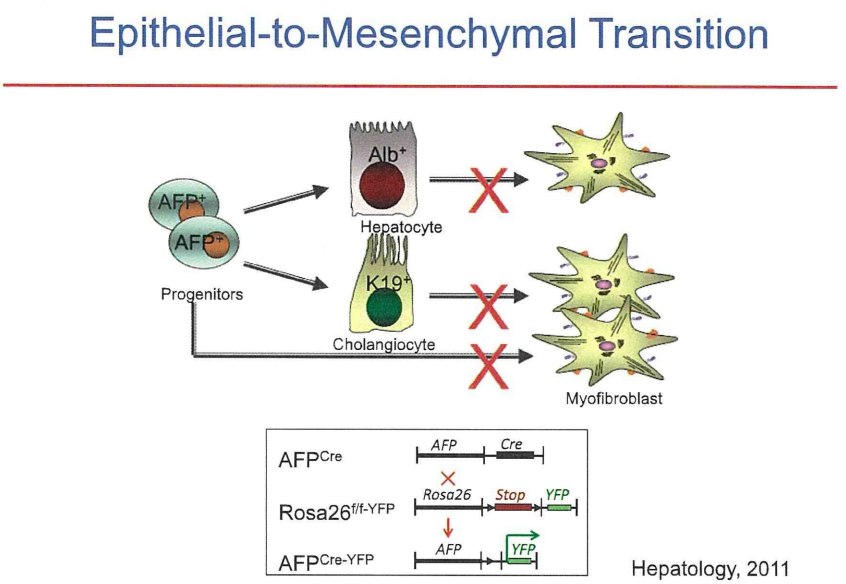

Figure 3 Analysis of epithelial-to-mesenchymal transition (EMT). (a) It is proposed that in EMT the myofibroblasts in liver fibrosis originate from hepatic epithelial cells, consisting of hepatocytes (albumin$^+$ [Alb$^+$] cells), cholangiocytes (cytokeratin-19$^+$ [K19$^+$] cells), or progenitor cells (AFP$^+$ cells). (b) Determining the origin of myofibroblasts using cell fate mapping. If a cell expressed α-fetoprotein (AFP), it will be irreversibly genetically labeled. AFP-driven Cre labeled epithelial progenitor cells, cholangiocytes, and hepatocytes, but failed to label any hepatic stellate cells (HSCs) or myofibroblasts. YFP, yellow fluorescent protein.[41]

BM stroma, do not express hematopoietic markers and can be isolated as Lin$^-$ CD45$^-$ CD31$^-$ CD34$^-$ CD133$^-$ Sca-1$^+$ Vitamin A$^-$ cells.[36,37] Whether BM-derived myofibroblasts contribute to ECM deposition in the course of liver fibrosis is unknown. In experimental liver fibrosis, only a small contribution of BM-derived cells to the myofibroblast population has been detected.[38]

Epithelial-to-mesenchymal transition

Epithelial-to-mesenchymal transition (EMT) is an important biological concept that describes the reversible transition of differentiated epithelial cells into mesenchymal cells with increased motility and changes in gene expression. Previous studies in the kidney and in the lung proposed that EMT occurs during fibrosis in those organs, and this concept was extrapolated to liver fibrosis.[39] Primary cell culture studies have clearly demonstrated that cholangiocytes and hepatocytes undergo a change in the phenotype and gene expression toward a mesenchymal cell, especially after incubation with transforming growth factor (TGF)-β, which is the cytokine most closely associated with EMT.[40] However, the more recent reports provide strong evidence against EMT in the liver as a source of myofibroblasts.[41] These studies use lineage tracing, such as by marking hepatic epithelial progenitor cells. Such mice are generated by crossing the α-fetoprotein (AFP) Cre mouse with the ROSA26YFP stop mouse to trace the fate of any cell ever expressing AFP. As expected, all cholangiocytes, hepatocytes, and oval cells were genetically labeled, because they are derived from a common AFP-expressing precursor cell. Furthermore, the critical result was that after inducing liver fibrosis by a variety of methods, none of the resulting myofibroblasts originated from the genetically marked epithelial (AFP$^+$) cells (Fig. 3).

Conclusions

Myofibroblasts are the source of the fibrous scar in liver fibrosis. Hepatic myofibroblasts are transdifferentiated from heterogeneous cell populations in response to variety fibrogenic stimuli. According to the most recent studies, the major sources of hepatic myofibroblasts in experimental liver fibrosis are hepatic stellate cells and portal fibroblasts. The role of EMT in liver fibrosis has been recently questioned. As a first approximation, myofibroblasts generated in hepatotoxic liver injury appear to originate from HSCs and myofibroblasts generated in cholestatic liver injury may originate from portal fibroblasts (Fig. 2).